International Journal of Structural Stability and Dynamics
(2024) 2450163 (29 pages)

DOI: 10.1142/S0219455424501633

Identification of Moving Vehicle Loads Using Instantaneous Vision-Based Vehicle Spatiotemporal Information and Improved Time Domain Method

Bohao Xu, Yuhan Chen and Ling Yu*

MOE Key Laboratory of Disaster Forecast and Control in Engineering
School of Mechanics and Construction Engineering
Jinan University, Guangzhou, P. R. China
**lyu1997@163.com*

Received 26 July 2023
Accepted 20 September 2023
Published 19 October 2023

Accurate identification of moving vehicle loads on bridges is one of the challenging tasks in bridge structural health monitoring, but lacks of intensive investigations to merge the heterogeneous data of vision-based vehicle spatiotemporal information (VVSI) and vehicle-induced bridge responses for moving force identification (MFI) in the existing time domain methods (TDM). In this study, a novel MFI method is proposed by integrating instantaneous VVSI and an improved TDM (iTDM). At first, a novel VVSI method combining background subtraction with template matching is presented to accurately track moving vehicles on bridges. With the calibration technique and camera perspective transformation model, the distribution of vehicles (DOV) on bridges is obtained and used as *a priori* information in the subsequent MFI. Then, the iTDM is developed based on the MFI equation re-formed in the form of instantaneous VVSI instead of the constant speed vehicle crossing bridges assumed in the traditional TDM. Finally, based on the redundant dictionary matrix composed of Haar functions for a moving load, the MFI problem is converted to explore a solution to the atom vectors and then solved by the Tikhonov regularization method. Experimental verifications in laboratory and a comparative study with the existing three methods are conducted to assess the feasibility of the proposed method. The results show that the proposed MFI method outperforms the existing methods and can effectively identify the moving vehicle loads with a higher and acceptable accuracy. It is successful for the proposed method to replace the assumption of constant speed vehicle crossing bridge in the traditional TDM with the instantaneous VVSI in the MFI problem.

Keywords: Moving force identification (MFI); vision-based vehicle spatiotemporal information (VVSI); vehicle–bridge interaction; redundant dictionary; Harr wavelet function; Tikhonov regularization.

*Corresponding author.

1. Introduction

Moving force identification (MFI), as one of the important issues in bridge structural health monitoring (BSHM), has been extensively paid attention in the last decades.[1,2] The accurate and stable identification of the vehicle loads moving across the bridge deck is of great significance to structural safety early warning and health monitoring of bridges.[3–5]

The modern MFI methodology can be classified into the direct and indirect methods. For the direct methods, the vehicle information, such as vehicle type, vehicle speed, axle number, axle-weight and gross vehicle weight (GVW), can be obtained directly by bridge weigh-in-motion system (BWIMs).[6] Nowadays, with the introduction of traffic video technology, vision-based vehicle spatiotemporal information (VVSI), such as vehicle speed, position, spatial distribution of vehicles (DOVs), etc., on the bridge deck can be obtained effectively.[7–12] However, it is necessary to guarantee the accuracy of the weight in motion (WIM) system by ensuring that the vehicle travels at a low speed, but this is unrealistic in the real traffic.[13] Furthermore, the DOV captured by the traffic video has a great impact on the subsequent MFI operation.

For the indirect methods, most of them tried to establish the relationship between moving forces and structural responses. They can be divided into four categories, such as the interpretive method I (IMI),[14] the interpretive method II (IMII),[15] the time domain method (TDM)[16] and the frequency-time domain method (FTDM).[17] Because the generation process of system matrix in TDM is clear and concise, many following studies tried to fix the ill-posedness in the MFI problem based on the TDM.[18] With the introduction of redundant dictionary theory, the MFI problem was converted into a sparse solution problem.[19–22] The choice of basis function in redundant dictionary has a great impact on the expression of the moving force.[21] The Haar wavelet functions, as one of the better choice of basis function, have been widely used in many fields and gained lots of achievements due to its best function approximation ability in time domain.[23] It has been applied to MFI and obtains the truck axle-weight successfully.[24] However, the dynamic components of the moving force and the acceleration response are ignored.

Besides, the above TDM methods assumed that the vehicle loads are moving across the bridge deck at a constant speed, which is unrealistic in practice. With the introduction of the VVSI, the vehicle positions can be used as *a priori* information to estimate the vehicle loads so that the assumption can be given up. Li *et al.*[25] obtained the vehicle positions by computer vision at first and used them as *a priori* information to establish the relationship between bridge responses and vehicle loads for obtaining the loads by a generalized Tikhonov regularization method indirectly. Wang *et al.*[26] proposed a novel vehicle load identification method according to machine vision and BP neural network to obtain speed, wheelbase and static weight of the vehicle. And there are some other vision-based methods proposed to

obtain the spatiotemporal information of the vehicle and even get the number of axle.[12,27] Li *et al.*[28] used another way which is based on an optimal combined strain influence line to obtain the axle information, transverse position of the load and the vehicle load. However, the acceleration responses mainly caused by the dynamic components of the vehicle loads are also ignored.

In view of these, a novel MFI method based on improved TDM (iTDM) is proposed using both instantaneous VVSI and vehicle-induced combined responses of bridges in this study. To detect the vehicle accurately, a novel VVSI method combining background subtraction with template matching methods is proposed at first. The DOV, which is obtained by Zhang's calibration technique[29] and camera perspective transformation model, is used as *a priori* information in the subsequent MFI. To combine with the VVSI method and the traditional TDM, the assumption that the speed of moving vehicle on the bridge deck is unchanged in the TDM is given up. The relationship between the moving forces and responses, namely, bending moment and acceleration responses, is established based on the *priori* information. The redundant matrix theory, which has been widely used in indirect methods, is introduced in this study. Due to the excellent performance of Haar functions, they are used to constitute the basis function in the redundant dictionary matrix. Finally, the Tikhonov method is used to obtain the solution to the MFI problem. Through these improvements, the MFI results have higher accuracy, and the dynamic components of moving forces can be accurately obtained.

The rest of this paper can be organized as follows: In Sec. 2, the proposed VVSI method is introduced. In Sec. 3, the theoretical background of the new MFI method is first proposed based on the VVSI and vehicle-induced combined responses of bridges, where the redundant dictionary matrix composed of Haar functions is used to represent the moving forces which are beneficial to the identification of dynamic components of moving forces, the final DOV and MFI results are then discussed and analyzed as well. Finally, several conclusions are drawn in Sec. 4. The flowchart of the proposed methods is shown in Fig. 1.

2. Vision-Based Vehicle Spatiotemporal Information Detection

In this section, the VVSI detection method is proposed based on the vision-based DOV data from the beam bridge in the laboratory, which serves as an illustration to showcase the procedure of the VVSI detection.

2.1. *Experimental preparation*

The following VVSI detection is carried out in the laboratory, as shown in Fig. 2, in which there are three beams, namely leading beam, main beam and trailing beam along the vehicle driving direction. Besides, an auxiliary beam is parallel to the main beam for fixing the photoelectric sensors and the calibration board establishing the

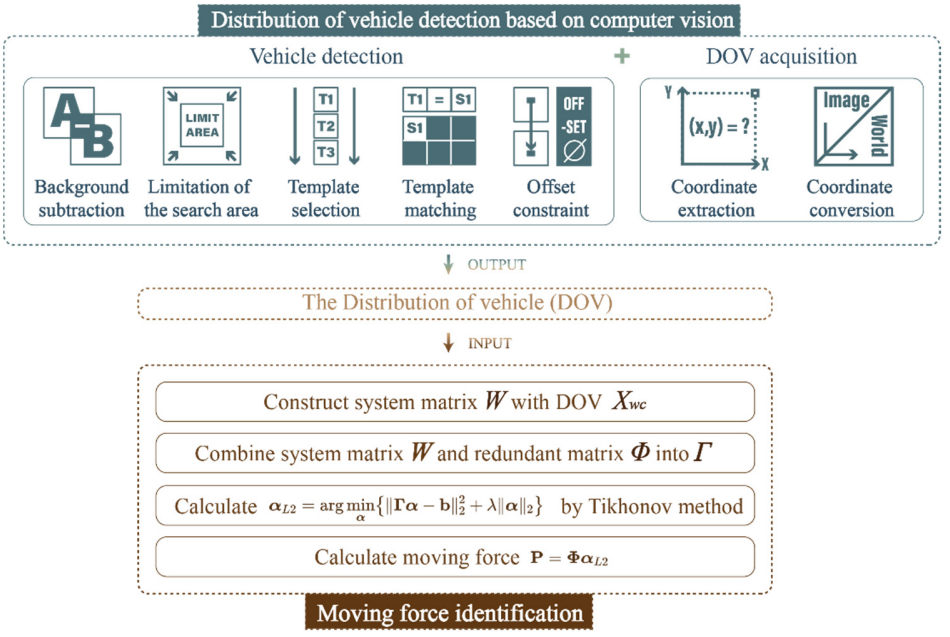

Fig. 1. Flow chart of proposed method.

image coordinates as shown in Fig. 2(a). A digital camera shown in Fig. 2(b) is installed above the trailing beam to capture the vehicle. The frame rate of the camera is 30 fps. The model vehicle as shown in Fig. 2(c) is subjected to motion through the action of a motor in Fig. 2(d) via a traction rope. The leading beam is used to accelerate the vehicle, and the trailing beam is used to slow down the vehicle until it stops. The length of the main beam is 3 m and features a hollow rectangular cross-section. Its width, height and wall thickness are 0.15 m, 0.05 m and 0.002 m, respectively. Three strain gauges and seven accelerometers equally-spaced installed under the bottom surface of the main beam are used to capture the vehicle-induced responses by the system of LMS Test.Lab.

2.2. *Vision-based DOV detection*

The fundamental theory of the background subtraction method is to subtract the reference background from the current foreground. In the grayscale image sequence from the video frames, an image without moving vehicles is chosen as a background $B(x, y)$. The foreground sequence $F_n(x, y)$ is the image containing moving vehicles. A grayscale subtraction image $D_n(x, y)$ containing moving vehicles is created by subtracting the background from the foreground frame sequence as follows:

$$D_n(x, y) = F_n(x, y) - B(x, y). \tag{2.1}$$

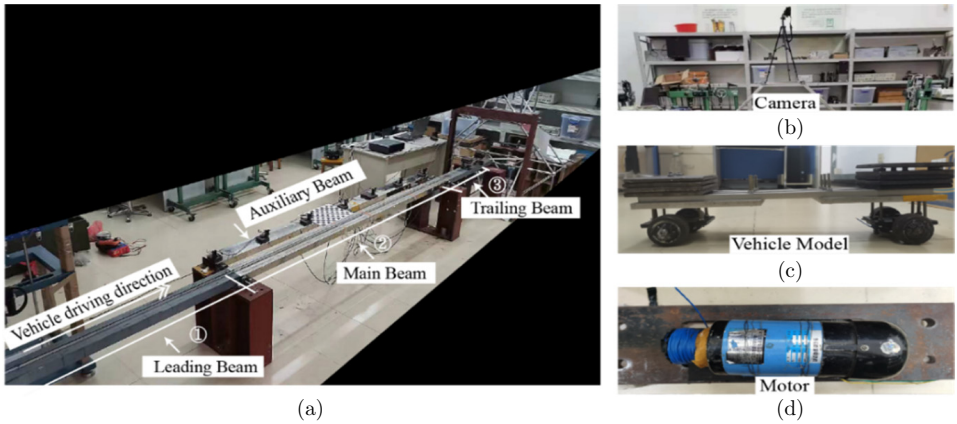

Fig. 2. Experimental layouts. (a) Setup in laboratory. (b) Camera. (c) Vehicle model. (d) Motor.

Template matching method in Chen *et al.*[8] provides us with fresh inspiration in the DOV detection. Furthermore, the template matching method can also group the vehicle into different categories automatically by the following improvements.[8] One is that a new parameter should be defined to distinguish the front of each identified vehicle, the other is that a database containing different vehicle types is established at the beginning. However, this method requires traversal computation of pixels and its computational cost is huge especially for large images. In this study, it is combined with the background subtraction method. This is because the external rectangle of the vehicle obtained by the background subtraction method provides *a priori* information to limit the searching area of template matching as shown in Fig. 3. It will decrease the computational cost of the traditional template matching method and reduce the influence of background interference.

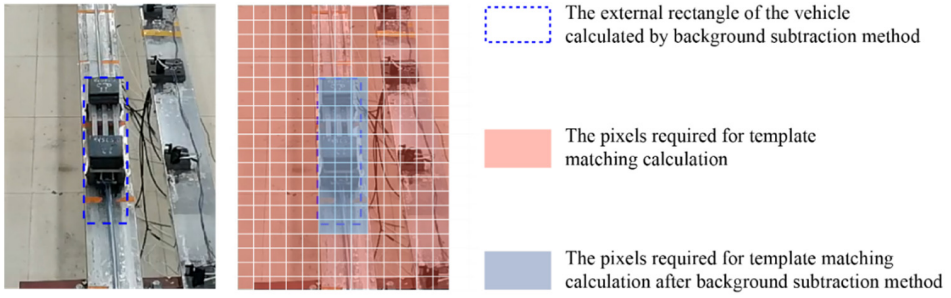

Fig. 3. Optimization of template matching by background subtraction in calculation.

Table 1. Results of virtual loop obtained according to different cases.

Case	Judgements		Results of the virtual loop
1	$A_n^{\text{on}} = 0$	$p_n^w < T_{\text{on}}$	Front axle has not arrived at the first virtual loop
2	$A_n^{\text{on}} = 1$	$p_n^w \geq T_{\text{on}}$	Front axle has arrived at the first virtual loop
3	$A_n^{\text{off}} = 1$	$p_n^w \leq T_{\text{off}}$	Rear axle has not left the second virtual loop
4	$A_n^{\text{off}} = 0$	$p_n^w > T_{\text{off}}$	Rear axle has left the second virtual loop

In this study, it is necessary to determine the precise times when the vehicle arrives at the bridge deck and leaves the bridge deck respectively in the DOV detection. Therefore, two areas located at the beginning and the end of the main beam are set to record these two moments. The virtual loops are introduced to indicate these areas and discussed separately when vehicles leave or arrive at the bridge. The arrival situations of vehicles are categorized into four cases as shown in Table 1.

When the front axle of the vehicle passes across the first virtual loop, the sub-image interception is performed, and the sub-image is used as the template. In the virtual loops, the number of white pixels p_n^w in the binarized image is compared with a pre-defined threshold T_{on} or T_{off} to determine whether the vehicle has arrived at or left the region. A_n^{on} or A_n^{off} is a property function that determines whether a vehicle is already on or off the bridge. When A_n^{on} or A_n^{off} equals one, the vehicles have arrived at (or left) the first virtual loop (or the second virtual loop) in the nth frame of the foreground image; otherwise, they have not. The above criterion can be written by mathematical expressions as follows:

$$A_n^{\text{on}} = \begin{cases} 1, & p_n^w \geq T_{\text{on}}, \\ 0, & p_n^w < T_{\text{on}}, \end{cases} \quad \text{or} \quad A_n^{\text{off}} = \begin{cases} 1, & p_n^w \leq T_{\text{off}}, \\ 0, & p_n^w > T_{\text{off}}, \end{cases} \tag{2.2}$$

The area for sub-image template interception is determined by the virtual loop, which is also considered as the area for the front axle of the vehicle. The sub-image template interception and updating is shown in Fig. 4. In Fig. 4(b), when the vehicle arrives at the first virtual loop, the system will collect and store the sub-image from the interception area and the corresponding sub-image will be used for template matching in the subsequent video frame. Furthermore, it can be found that the vehicle in the video data will become larger when it moves closer to the camera. Therefore, the sub-image will be updated when the vehicle goes through each marked area as shown in Figs. 4(b) and 4(c). After feature extraction, the bounding box in the nth frame foreground image intersects with the marked areas, the sub-image template is updated. The foreground image in the $(n+1)$th frame is matched according to the updated sub-image template.

The template matching based on the grayscale values as shown in Fig. 5 is used to compare the template T on the foreground image with the sub-image I for obtaining the interested area. In this study, the zero-normalized cross-correlation

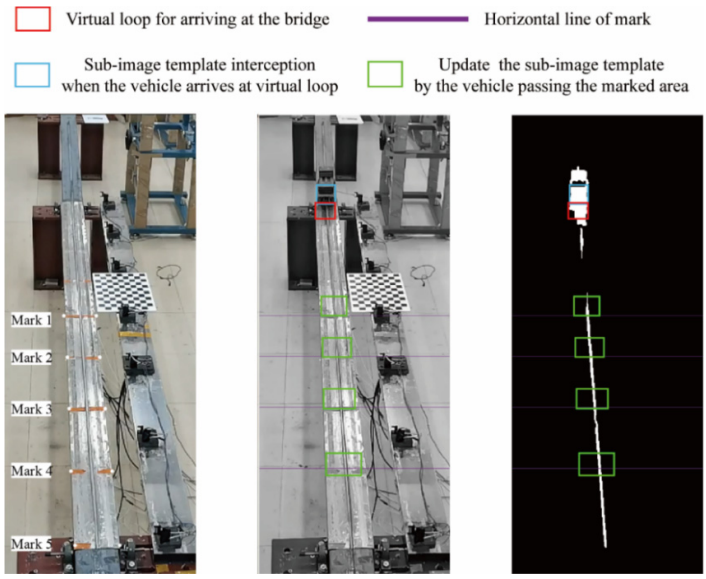

Fig. 4. Sub-image template interception and updating. (a) Schematic diagram of bridge marker distribution. (b) Area distribution for sub-image template interception and updating in grayscale image. (c) Area distribution for sub-image template interception and updating in binary image.

(ZNCC) as shown in Fig. 5(a) is introduced to measure the similarity of $R_n(u,v)$ grayscale intensities between the template T and sub-image I. It can be written as

$$R_n(u,v) = \frac{\mathrm{cov}(T,I)}{\sigma_T \sigma_I} = \frac{\sum_{x,y}[T(x,y) - u_T] \cdot [I(u+x, v+y) - u_I]}{\sqrt{\sum_{x,y}[T(x,y) - u_T]^2 \cdot [I(u+x, v+y) - u_I]^2}}, \tag{2.3}$$

where (u,v) and (x,y) are the foreground image and sub-image template coordinates, respectively. u_T and u_I represent the mean intensities of the template and sub-image in the foreground image at (u,v), respectively. $\mathrm{cov}(T,I)$ is the covariance matrix of template T and sub-image I. σ_T and σ_I represent the variance of template T and sub-image I, respectively.

As the template slides through the whole foreground image in units of pixel length, the similarity of all pixels is calculated. Then, the maximum similarity of the current frame MR_n is calculated as,

$$\mathrm{MR}_n = \max R_n(u,v). \tag{2.4}$$

The bounding box is formed in the foreground picture of the current frame, and its position is related to the MR_n as shown in Fig. 5(b).

However, after the sub-image template is obtained, the interference would perhaps occur when the background and the sub-image have similar gray intensities. As a result, the bounding box in the next frame will move into the background

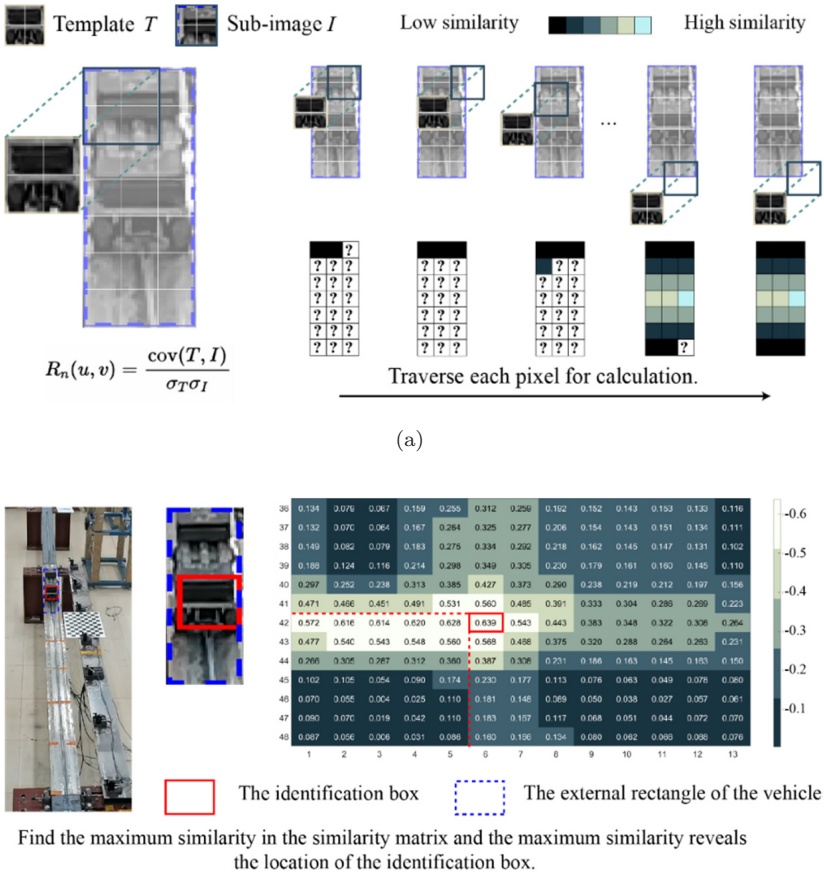

Fig. 5. Template matching algorithm based on grayscale. (a) ZNCC. (b) Maximum similarity and corresponding bounding box.

areas and will eventually confuse the identification. It is necessary to set an offset constraint as shown in Fig. 6. The offset constraint relies on the camera height, camera frame rate and vehicle speed. The vehicle speed is a main factor which is always ignored. When the vehicle moves across a bridge at a high speed, its offset in inter-frame bounding box is large. So the vehicle is controlled to move at a high speed to determine this offset constraint. The camera height and frame rate can be determined in the preparation of the experiment. Finally, the predetermined offset threshold is 15 pixels in this study.

As shown in Fig. 6(a), a correct bounding box will produce a modest offset in the vertical direction of the image between each frame. Furthermore, the vertical offset

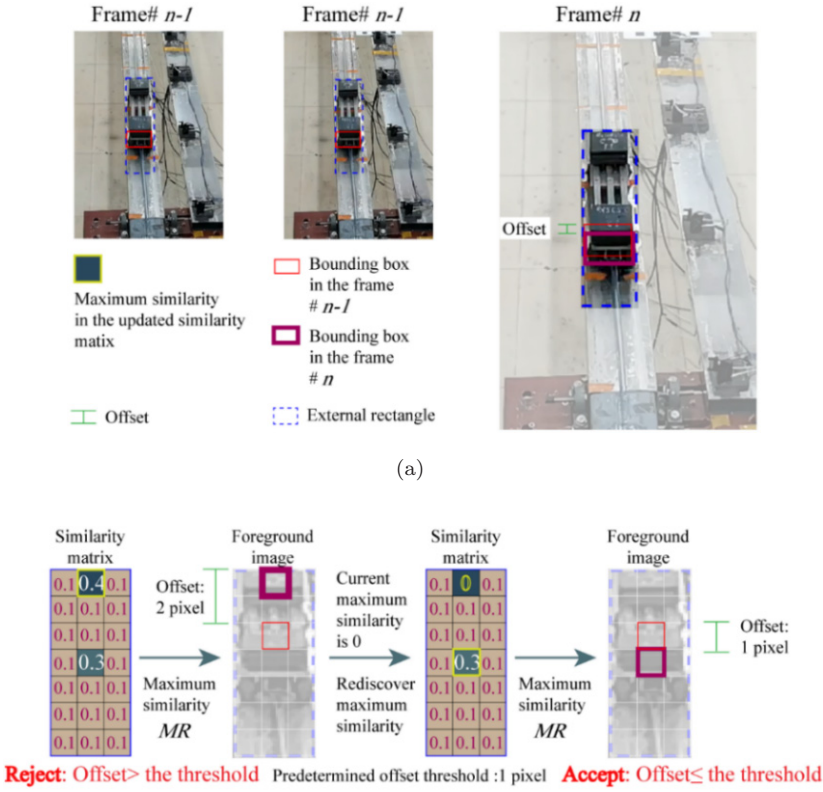

Fig. 6. Offset constraint. (a) Vertical offset in inter-frame bounding box. (b) Process of offset constraint.

is constrained by a preset threshold. As shown in Fig. 6(b), when the offset exceeds the threshold, the bounding box is misidentified and the maximum similarity of the current frame MR_n is assigned as 0. Then the MR_n and the corresponding bounding box will be rediscovered until the correct identification is completed. It should be noted that different cameras with different positions and angles have an impact on the selected template in the proposed method. So it needs to make sure that the vehicle front can be detected during the whole time.

2.3. *DOV detection via coordinate extraction*

Firstly, the coordinate extraction is performed as shown in Fig. 7. After obtaining the bounding box, the midpoint of the bottom edge is considered as the vehicle front axle position after the bounding box is obtained as shown in Fig. 7(a). The detection results in the first axle as shown in Fig. 7(b) are near the bridge centerline.

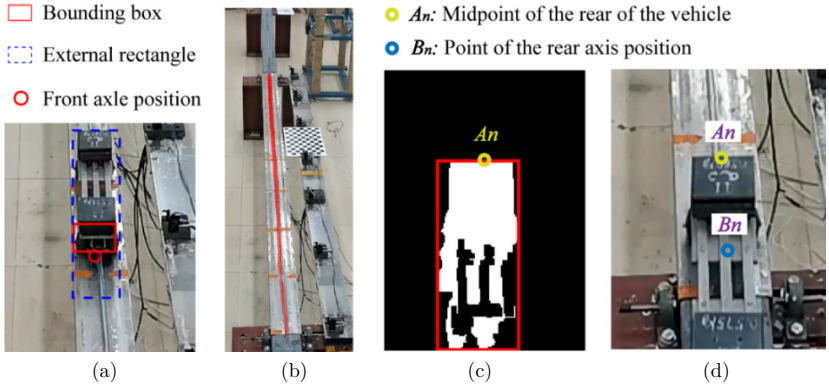

Fig. 7. Coordinate extraction. (a) Extraction of front axle coordinates when vehicle enters the bridge. (b) Distribution of front axle coordinate in foreground sequence images. (c) Coordinate extraction of rear axle of vehicle captured by background subtraction method. (d) Schematic diagram of coordinate selection of A_n and B_n.

Furthermore, the position of the rear axle can be identified if the vehicle type is known.

However, once the front axle of the vehicle exits the bridge, the camera cannot capture the frontal image of the vehicle anymore because of the constraint of the camera field of view (FOV). Template matching is no longer appropriate in this situation. Therefore, based on the vehicle reference, a function fitting method basis is proposed to extract the instantaneous coordinates of the vehicle position. At first, some frame images are picked to get the coordinates of the rear axle by obtaining the vehicle external rectangular box in the background subtraction method. For the nth foreground image, the midpoint $A_n(x_{An}, y_{An})$ of the rear of vehicle can be captured by the background subtraction method as shown in Fig. 7(c). As shown in Fig. 7(d), the position of the rear axle in the nth foreground image is artificially selected as $B_n(x_{Bn}, y_{Bn})$. It is assumed that the coordinates of each frame point exhibit a linear relation between A_n and B_n. Therefore, a linear fitting function between A_n and B_n can be established. Thus, the position of the rear axle can be captured through A_n.

To convert the vehicle pixel coordinates $[u, v, 1]^T$ to the actual world coordinates $[x_{\mathrm{wc}}, y_{\mathrm{wc}}, z_{\mathrm{wc}}, 1]^T$, the camera perspective projection model can be created and expressed in the matrix form as

$$Z_c \begin{Bmatrix} u \\ v \\ 1 \end{Bmatrix} = \begin{bmatrix} 1/dx_{\mathrm{im}} & 0 & u_0 \\ 0 & 1/dy_{\mathrm{im}} & v_0 \\ 0 & 0 & 1 \end{bmatrix} \begin{bmatrix} f_c & 0 & 0 & 0 \\ 0 & f_c & 0 & 0 \\ 0 & 0 & 1 & 0 \end{bmatrix} \begin{bmatrix} R_{3\times3} & T_{3\times1} \\ 0 & 1 \end{bmatrix} \begin{Bmatrix} x_{\mathrm{wc}} \\ y_{\mathrm{wc}} \\ z_{\mathrm{wc}} \\ 1 \end{Bmatrix}, \quad (2.5)$$

where dx_{im} and dy_{im} are the unit scale factors. u_0 and v_0 are the shift values connecting the origins of two coordinate systems. f_c is focal length. $R_{3\times3}$ and $T_{3\times1}$ are a rotation matrix with a dimension of 3×3 and a shift vector with a dimension of 3×1, respectively.

Zhang's calibration technique[26] is utilized to get the parameter matrix. Therefore, the coordinates $[u, v, 1]^T$ extracted from the pixel coordinate system can be transformed to obtain the coordinate $[x_{\text{wc}}, y_{\text{wc}}, z_{\text{wc}}, 1]^T$ in the world coordinate system. After coordinate extraction and transformation, the coordinates of the vehicle axles P_{Axle} at time t_{ci} can be written as:

$$P_{\text{Axle}}(t_{ci}) = \left[x_{\text{wc}}(t_{ci}), y_{\text{wc}}(t_{ci}), z_{\text{wc}}(t_{ci})\right], \quad i = 0, 1, 2, \ldots, N_c, \tag{2.6}$$

where $N_c + 1$ is the number of sampling points by the camera.

In the FOV of the camera, the bridge deck is a planar pattern and its elevation would not change greatly. Therefore, z_{wc} can be regarded as a constant.[6] In addition, this study mainly discusses the DOV along the longitudinal direction of the bridge. If $y_{\text{wc}} = z_{\text{wc}} = 0$, the coordinates of $x_{\text{wc}}(t_{ci})$, i.e. the vehicle position along the longitudinal direction of the bridge can be represented by the coordinates of vehicle $P_{\text{Axle}}(t_{ci})$ as written in the following equation:

$$x_{\text{wc}}(t_{ci}) = P_{\text{Axle}}(t_{ci}), \quad i = 0, 1, 2, \ldots, N_c. \tag{2.7}$$

In short, the proposed VVSI detection method is achieved through the vision-based DOV detection mentioned here, which includes three steps, i.e. background subtraction, template matching and coordinate extraction as mentioned above. The provided instantaneous coordinate information of the vehicle axles will be used as the *priori* information in the subsequent MFI for determining the moving vehicle loads.

2.4. *Preprocessing of measured data fusion*

It is noteworthy that the response sensors and video camera should be time-synchronized so that the instantaneous vehicle positions and vehicle-induced response data can be recorded simultaneously. The frame rate of camera is always much less than the sampling frequency of the measured responses. As usual, the sampling frequency is a few multiples of the frame rate of camera so that it is easy to find a relationship between them.[30] However, the sampling frequency of response data is usually set as the power of two for easy data storage and analysis. The vision-based DOV data directly obtained at the frame rate of the camera do not match the data collected at the sampling rate of measured responses. Furthermore, the frame rate of the camera is enough for the MFI solution if only the static weights of moving forces are needed in the previous study. However, the dynamic components of moving forces dominated in the higher frequency domain are also of concern in

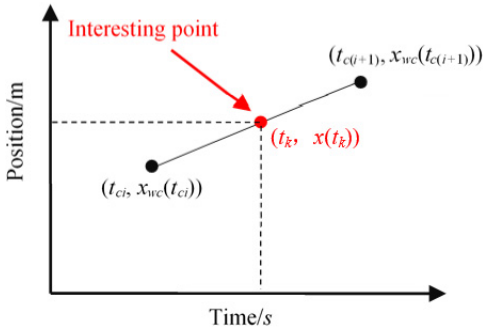

Fig. 8. Fitting function of data fusion.

this study. Therefore, the frame rate of the camera is not enough for the lowest sampling frequency of response data according to the Shannon sampling theorem.

In this study, the vehicle speed between two adjacent frames is assumed as unchanged. Here, $x_{\mathrm{wc}}(t_{ci})$ is the collected frame by the camera at time t_{ci}, $x(t_k)$ is the measured data collected at the interested sampling rate at time t_k as shown in Fig. 8. If an interested point is between two adjacent frames, then $x(t_k)$ can be obtained by

$$x(t_k) = x_{\mathrm{wc}}(t_{ci}) + \frac{x_{\mathrm{wc}}(t_{c(i+1)}) - x_{\mathrm{wc}}(t_{ci})}{t_{c(i+1)} - t_{ci}}(t_k - t_{ci}),$$
$$i = 0, 1, 2, \ldots, N_c, \quad k = i = 0, 1, 2, \ldots, N_m, \tag{2.8}$$

where $N_c + 1$ and $N_m + 1$ are the numbers of collected frames by the camera and of measured response data, respectively.

Then the instantaneous positions of each vehicle axle matched with response data at the interested sampling frequency are used for the MFI calculation in the next section.

3. Moving Force Identification Combining VVSI and Vehicle-Induced Responses of Bridges

3.1. *MFI equation represented by instantaneous VVSI in time domain*

As a classical MFI method, TDM has established the relationship between structural responses and moving vehicle loads in time domain, and there are some important assumptions made. One is that the mass ratio between two-axle vehicle and bridge is lower so that a vehicle crossing a bridge can be considered as two moving forces on the bridge deck. The other assumes that the moving vehicle moves across the bridge at a constant velocity of cc as presented in Fig. 9. In this study, the first

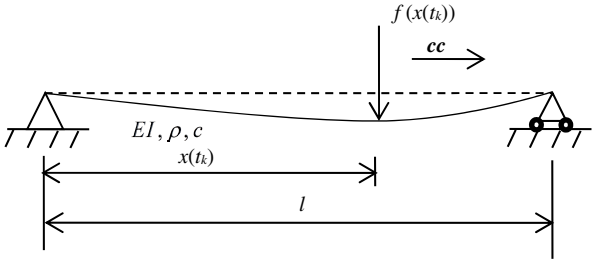

Fig. 9. A simply supported beam subjected to a moving force.

assumption still holds here, but the second assumption is completely given up since the constant vehicle speed is not the fact in site but is instantaneously variable. If the vehicle speed is multiplied by the time, it will be transformed to the instantaneous vehicle position directly, which can be obtained by the VVSI detection in the preceding section. As shown in Fig. 9, a simply supported beam subjected to a moving force $f(x(t_k))$, which is at the position $x(t_k)$, is taken as an example to establish a relationship between moving forces and structural responses, where EI, c, ρ and l are the flexural stiffness, viscous damping, mass per unit length and span of the beam, respectively.

Based on the modal superposition principle and the convolution integral, the bending moment and acceleration responses can be re-formed by

$$m(x,t_k) = \sum_{n=1}^{\infty} \frac{-2EI}{\rho l \omega_n'} \Phi_n''(x) \sum_{k_1=0}^{k} e^{-\xi_n \omega_n \Delta t(k-k_1)} \sin \omega_n' \Delta t(k-k_1) \Phi_n(x(t_k)) \times f(x(t_k)) \Delta t, \tag{3.1}$$

$$a(x,t_k) = \sum_{n=1}^{\infty} \frac{2}{\rho l \omega_n'} \Phi_n(x) \left[\Phi_n(x(t_k)) f(x(t_k)) + \sum_{k_1=0}^{k} \chi_n(k\Delta t - k_1 \Delta t) \Phi_n(x(t_{k_1})) \times f(x(t_{k_1})) \Delta t \right], \tag{3.2}$$

where $\Phi_n(x)$, ω_n, $\xi_n = c/2\rho\omega_n$ and $\omega_n' = \omega_n\sqrt{1-\xi_n^2}$ are the nth modal shape function, modal frequency, damping ratio and damped modal frequency, respectively. Δt is the sampling interval, $\chi_n(t) = [(\xi_n^2\omega_n^2 - \omega'^2{}_n)\sin\omega_n' t - 2\xi_n\omega_n\omega_n' \cos\omega_n' t]e^{-\xi_n\omega_n t}$. For convenience of the following MFI calculation, Eqs. (3.1) and (3.2) can be transformed into a matrix form. Here, the numbers of the sampling points of measured responses and moving forces are $N+1$ and N_m+1, respectively. Assuming that there is no moving force imposing on the beam before the moving force enters and

after exits the beam, Eq. (3.1) can be rewritten in a matrix form

$$\begin{bmatrix} m(x,2) \\ m(x,3) \\ \vdots \\ m(x,N) \end{bmatrix} = \sum_{n=1}^{\infty} \mathrm{M}_{xn} \begin{bmatrix} Q_{mn}(1)X_n(1) & 0 & \cdots & 0 \\ Q_{mn}(2)X_n(1) & Q_{mn}(1)X_n(2) & \cdots & 0 \\ \vdots & \vdots & \vdots & \vdots \\ Q_{mn}(N-1)X_n(1) & Q_{mn}(N-2)X_n(2) & \cdots & Q_{mn}(1)X_n(N_m-1) \end{bmatrix} \times \begin{bmatrix} f(x(t_1)) \\ f(x(t_2)) \\ \vdots \\ f(x(t_{N_m-1})) \end{bmatrix}, \tag{3.3}$$

where $M_{xn} = -2EI\Phi_n''(x)/\rho l\omega_n'$, $Q_{mn}(k) = e^{-\xi_n\omega_n k\Delta t}\sin\omega_n' k\Delta t$ and $X_n(k) = \Phi_n(x(t_k))$.

Similarly, Eq. (3.2) can be also rewritten in a matrix form,

$$\begin{bmatrix} a(x,1) \\ a(x,2) \\ \vdots \\ a(x,N) \end{bmatrix} = \sum_{n=1}^{\infty} A_{xn} \begin{bmatrix} (1+Q_{an}(0))X_n(1) & 0 & \cdots & 0 \\ Q_{an}(1)X_n(1) & (1+Q_{an}(0))X_n(2) & \cdots & 0 \\ \vdots & \vdots & \vdots & \vdots \\ Q_{an}(N-1)X_n(1) & Q_{an}(N-2)X_n(2) & \cdots & Q_{an}(1)X_n(N_m-1) \end{bmatrix} \times \begin{bmatrix} f(x(t_1)) \\ f(x(t_2)) \\ \vdots \\ f(x(t_{N_m-1})) \end{bmatrix}, \tag{3.4}$$

where $A_{xn} = 2\Phi_n(x)/\rho l\omega_n'$ and $Q_{an}(k) = \Delta t\chi_n(t_k)$.

From Eqs. (3.3) and (3.4), it can be found that the biggest difference between them and the classical TDM is that the position of the moving force is directly written in X_n in each system matrix. Furthermore, the elements in the moving force vector are related to the instantaneous positions of vehicles. Therefore, this developed way is called an improved time domain method (iTDM) in distinction from the classical TDM.

Then, Eqs. (3.3) and (3.4) can be combined and rewritten as follows:

$$\mathbf{W}\mathbf{f} = \mathbf{b}, \tag{3.5}$$

where $\mathbf{f}$ is the vector of moving forces, $\mathbf{b}$ is the vector of structural responses and $\mathbf{W}$ is the system matrix between moving forces and structural responses, respectively.

The procedure outlined above is designed to identify a single force. With the linear superposition principle, Eq. (3.5) can be modified as the following equation to identify two moving forces:

$$\begin{bmatrix} \mathbf{W}_a & \mathbf{0} \\ \mathbf{W}_b & \mathbf{W}_c \\ \mathbf{W}_d & \mathbf{W}_e \end{bmatrix} \begin{Bmatrix} \mathbf{f}_1 \\ \mathbf{f}_2 \end{Bmatrix} = \mathbf{b}, \tag{3.6}$$

where $\mathbf{W}_a[N_{s1} \times (N_{m1} - 1)]$, $\mathbf{W}_b[(N - 1 - N_{s1} - N_{s2}) \times (N_{m1} - 1)]$, $\mathbf{W}_c[(N - 1 - N_{s1} - N_{s2}) \times (N_{m2} - 1)]$, $\mathbf{W}_d[N_{s2} \times (N_{m1} - 1)]$ and $\mathbf{W}_e[N_{s2} \times (N_{m2} - 1)]$ are sub-matrixes of $\mathbf{W}$. Each row of these sub-matrixes has the same meaning as in Ref. 16, but the dimensions of each sub-matrixes are different from the one in it. N_{s1} is the number of the sampling points when the first axle is on the bridge but the second axle is not on it. N_{s2} is the number of the sampling points when the second axle is on the bridge but the first axle is not on it. N_{mi} is the number of the sampling points for each force. If the velocity of the vehicle is unchanged, N_{s1} are equal to N_{s2} and N_{mi} of each force is equal to each other.

When the acceleration responses and bending moments are both used in the MFI calculation, their magnitudes need to be normalized into the same-class level, as follows:

$$\begin{bmatrix} \mathbf{W}_{11}/\|\mathbf{b}_1\| & \mathbf{W}_{12}/\|\mathbf{b}_1\| & \cdots & \mathbf{W}_{1n_f}/\|\mathbf{b}_1\| \\ \mathbf{W}_{21}/\|\mathbf{b}_2\| & \mathbf{W}_{22}/\|\mathbf{b}_2\| & \cdots & \mathbf{W}_{2n_f}/\|\mathbf{b}_2\| \\ \vdots & \vdots & \vdots & \vdots \\ \mathbf{W}_{n_r1}/\|\mathbf{b}_{n_r}\| & \mathbf{W}_{n_r2}/\|\mathbf{b}_{n_r}\| & \cdots & \mathbf{W}_{n_rn_f}/\|\mathbf{b}_{n_r}\| \end{bmatrix} \begin{Bmatrix} \mathbf{f}_1 \\ \mathbf{f}_2 \\ \vdots \\ \mathbf{f}_{n_f} \end{Bmatrix} = \begin{Bmatrix} \mathbf{b}_1/\|\mathbf{b}_1\| \\ \mathbf{b}_2/\|\mathbf{b}_2\| \\ \vdots \\ \mathbf{b}_{n_r}/\|\mathbf{b}_{n_r}\| \end{Bmatrix}, \tag{3.7}$$

where n_r and n_f are the number of both the responses and the moving forces, respectively.

3.2. *Moving force representation using redundant dictionary matrix composed of Haar functions*

In fact, the moving force $\mathbf{f}$ can be further expressed by a redundant matrix $\mathbf{\Phi}$,[19]

$$\mathbf{f} = \mathbf{\Phi}\boldsymbol{\alpha}, \tag{3.8}$$

where $\boldsymbol{\alpha}$ is the atom vector of redundant matrix $\mathbf{\Phi}$.

It should be noted that the form of redundant matrix has a great impact on the moving force expression.[21] According to the *priori* knowledge, the moving force is usually assumed to be composed of static and dynamic components, where the static component was described by a constant vector and the dynamic components were described by dictionaries composed of Level-1 Haar scaling functions and Level-1 Haar wavelet functions.[24] Due to their best function approximation ability in time domain, they are also adopted to construct the redundant matrix in this study. For the convenient MFI calculation, the Haar functions need to be expressed discretely in a matrix form. Their discrete forms can be obtained by sampling it at a power of two.[31] In the Hilbert space, they constitute an independent set of functions.[32] If $\mathbf{\Phi}_s$ is a dictionary composed of the Level-1 Haar scaling functions and $\mathbf{\Phi}_w$ is a dictionary composed of the Level-1 Haar wavelet functions, they can be expressed as follows:

$$\mathbf{\Phi}_s = \begin{bmatrix} 1 & 0 & \cdots & 0 \\ 1 & 0 & \cdots & 0 \\ 0 & 1 & \cdots & 0 \\ 0 & 1 & \cdots & 0 \\ \vdots & \vdots & \cdots & \vdots \\ 0 & 0 & \cdots & 1 \\ 0 & 0 & \cdots & 1 \end{bmatrix}, \quad \mathbf{\Phi}_w = \begin{bmatrix} 1 & 0 & \cdots & 0 \\ -1 & 0 & \cdots & 0 \\ 0 & 1 & \cdots & 0 \\ 0 & -1 & \cdots & 0 \\ \vdots & \vdots & \cdots & \vdots \\ 0 & 0 & \cdots & 1 \\ 0 & 0 & \cdots & -1 \end{bmatrix}. \tag{3.9}$$

From Eq. (3.9), it can be found that each column, which is also the basis function, in $\mathbf{\Phi}_s$ and $\mathbf{\Phi}_w$ is orthogonal to each other. Furthermore, every column in $\mathbf{\Phi}_s$ is also orthogonal to every column in $\mathbf{\Phi}_w$. Therefore, they strictly satisfy the requirement of the basis function in the redundant matrix. If only one moving force is considered, the number n_b of the basis functions in $\mathbf{\Phi}_s$ and $\mathbf{\Phi}_w$ is equal to the dimension of the moving force vector $N_m - 1$. Then, if $\mathbf{\Phi}_c$ is a constant vector, the redundant matrix in this study can be expressed as

$$\mathbf{\Phi} = [\mathbf{\Phi}_c \ \mathbf{\Phi}_s \ \mathbf{\Phi}_w]. \tag{3.10}$$

The number of basis functions in Eq. (3.10) is $2 \times N_m - 1$ and it satisfies the dimension requirements of redundant matrix whose number of the basis function is larger than the dimension of the original signal.

Substituting Eq. (3.8) into Eq. (3.5), the MFI problem is transformed into an atom vector recovery problem

$$\mathbf{W}\boldsymbol{\Phi}\boldsymbol{\alpha} = \mathbf{b}. \tag{3.11}$$

For brevity, if $\boldsymbol{\Gamma} = \mathbf{W}\boldsymbol{\Phi}$, Eq. (3.11) is rewritten as

$$\boldsymbol{\Gamma}\boldsymbol{\alpha} = \mathbf{b}. \tag{3.12}$$

According to the fact that the collected structural responses of $\mathbf{b}$ easily suffer from the measurement noise in practice, the atom vector $\boldsymbol{\alpha}$ is easy to be polluted and hard to express the moving forces greatly. In Ref. 24, Eq. (3.12) was solved by reweighted l_1-norm regularization technique, but only the bending moments dominated in a low-frequency domain were used for MFI. In fact, acceleration responses include higher frequency information beneficial to the identification of dynamic components of moving forces, they are easily measured in the site and also for concerning issues in this study. Because the Haar functions are discretely and uniformly distributed in time domain and the Tikhonov method can provide a dense solution,[33] the dynamic components of moving forces in each position of the vehicle on the bridge can be accurately obtained.[34] Then Eq. (3.12) is solved by

$$\boldsymbol{\alpha}_{L2} = \arg\min_{\boldsymbol{\alpha}}\{\|\boldsymbol{\Gamma}\boldsymbol{\alpha} - \mathbf{b}\|_2^2 + \lambda\|\boldsymbol{\alpha}\|_2\}, \tag{3.13}$$

where λ is a regularization parameter and is obtained by the L-curve method.[35] After obtaining the atom vector $\boldsymbol{\alpha}$, the moving forces $\mathbf{f}$ can be obtained by substituting the atom vector $\boldsymbol{\alpha}$ into Eq. (3.8).

4. Experimental Verifications

4.1. *Experimental setup*

In this study, a hollow beam bridge as shown in Fig. 2 is taken to validate the proposed method. The main beam has a unit length density ρ of 7.62 kg/m and a flexural rigidity EI of $7.94\times10^4\,\mathrm{N\cdot m^2}$. Because the ideal hinged supports are difficult to attain and there are also uncertainties in the bridge materials, an experimental modal analysis (EMA) is first carried out for obtaining the modal characteristics of the bridge, which are used to update the finite element model (FEM) of the bridge as well as to assess the supporting conditions of the bridge. The FEM in Ref. 36 is the basis for this study, and its first three frequencies are 19.56, 73.09 and 162.30 Hz, respectively. Besides, the first three damping ratios are 1.41%, 1.44% and 0.58%, respectively.

The relationship between the measured strains and related bending moments calculated by the updated FEM should be established. Five-level masses are located at the positions of the installed strain gauges successively. Finally, the coefficients of the strain gauges at 1/4, 1/2 and 3/4 spans are determined as $2.849\,\mathrm{N\cdot m\cdot}\mu\varepsilon^{-1}$,

Table 2. VVSI detection cases under different axle weights and mean speeds.

Cases	Mean speed/m/s	Front axle/kg	Rear axle/kg	GVW/kg
1	1.3796	5.5671	5.5717	11.1388
2	1.3289	4.9669	6.7741	11.7410
3	1.3766	6.6510	5.1842	11.8352

$2.813\,\mathrm{N}\cdot\mathrm{m}\cdot\mu\varepsilon^{-1}$ and $3.065\,\mathrm{N}\cdot\mathrm{m}\cdot\mu\varepsilon^{-1}$, respectively. A low-pass Butterworth filter is used to filter all the measured responses acquired at a sampling rate of 1 024 Hz. Since only the first three modal data are used in this study, all the filtered responses are resampled at a sampling rate of 512 Hz for easy storage and calculation in MFI.

4.2. *Experimental results and analysis*

4.2.1. *VVSI detection*

In this section, the vehicle–bridge model as shown in Fig. 2 is employed. To perform the VVSI detection, Table 2 lists the different cases set for the model vehicle. The data from Fig. 10 indicates the instantaneous positions of vehicle axles in video frame sequences under Case 1, where the red and blue circles represent the spatiotemporal information of the front axle and rear axle, respectively.

In Fig. 10, the whole process data on vehicle crossing the bridge deck can be intercepted to zoom in and obtain the spatiotemporal information of the vehicle axles at the precise moment when the vehicle enters and exits the bridge deck. The corresponding instants when the vehicle enters and exits the bridge deck are determined as in Table 3 under all the cases.

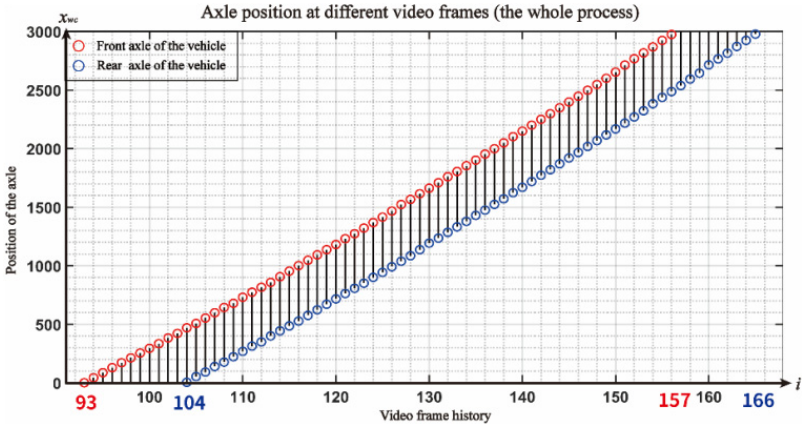

Fig. 10. Positions of vehicle axles in video frame sequences under Case 1.

Table 3. Instants when vehicle enters and exits bridge.

Cases	Entering bridge (unit: frame) Front axle [Rear axle]	Exiting bridge (unit: frame) Front axle [Rear axle]
1	93 [104]	157 [166]
2	75 [91]	188 [200]
3	58 [66]	123 [130]

In order to validate the accuracy of the proposed VVSI detection method, seven photoelectric sensors are also attached along an auxiliary beam parallel to the main beam as shown in Fig. 2. When two cantilever strips fixed over two vehicle axles sweep seven photoelectric sensors, the impulsive signals of sampling points will be produced and acquired by the LMS Test.Lab system. The corresponding spatiotemporal information of vehicle axles will be also recorded by the camera simultaneously. Then the accuracy of the proposed VVSI method can be calculated by the relative time error (RTE) between the acquired point sequences and image frame sequence.

For the front axle of the vehicle, the sequence number of sampling points $\mathrm{SP}_1, \mathrm{SP}_2, \ldots, \mathrm{SP}_6, \mathrm{SP}_7$ and sequence number of frames $\mathrm{FR}_1, \mathrm{FR}_2, \ldots, \mathrm{FR}_6, \mathrm{FR}_7$ are determined, respectively, when the vehicle passes through the seven photoelectric sensors. Relative sampling points D_{SPi} and relative frames D_{FRi} are both used to describe the amount of sampling points and frames captured when the vehicle passes through the first photoelectric sensor to the ith photoelectric sensor, respectively. The time required in the process T_{SPi} and T_{FRi} can be both calculated through the sampling frequency of photoelectric sensors f_{SP} and f_{camera}, respectively. The process can be expressed by the following equations:

$$\begin{cases} D_{SPi} = \mathrm{SP}_i - \mathrm{SP}_1, \\ T_{SPi} = D_{SPi}/f_{\mathrm{SP}}, \end{cases} \quad \begin{cases} D_{FRi} = \mathrm{FR}_i - \mathrm{FR}_1, \\ T_{FRi} = D_{FRi}/f_{\mathrm{camera}}, \end{cases}, \quad i = \{1, 2, 3, 4, 5, 6, 7\}. \tag{4.1}$$

To evaluate the accuracy of the proposed VVSI detection method, RTE between the T_{SPi} and T_{FRi} in the i-th photoelectric sensor is defined as:

$$RTE_i = \frac{|T_{FRi} - T_{SPi}|}{T_{SPi}} \times 100\%. \tag{4.2}$$

The results on RTE_i under three cases in Table 2 are shown in Table 4. One can find from Table 4 that the VVSI detection method can effectively detect the instantaneous positions of the front and rear vehicle axles under all the cases with acceptable accuracy. However, it can be also found from Table 4 that when the vehicle arrives s^{t}7th photoelectric sensor, the RTE is larger than that at the other photoelectric sensors. The reasons may be as follows: (1) When the vehicle approaches the trailing beam at a higher speed, the pulling motor of the vehicle will have to tune off for stopping the vehicle immediately due to the limited length of the trailing beam, this operation has a certain influence on the accuracy of VVSI detection.

Table 4. Results of RTE_i under all cases.

Case	i	$\mathrm{SP}_i[D_{SPi}]$	T_{SPi}/s	$\mathrm{FR}_i[D_{FRi}]$	T_{FRi}/s	RTE_i
	1	9 203	—	93	—	—
	2	10 015 [812]	0.39648	104	0.37457	2.19%
	3	10 796 [1 593]	0.77783	116	0.78319	0.53%
1	4	11 560 [2 357]	1.15088	127	1.15776	0.69%
	5	12 220 [3 017]	1.47314	136	1.46423	0.89%
	6	12 960 [3 757]	1.83447	147	1.83880	0.43%
	7	13 691 [4 488]	2.19141	157	2.17932	1.21%
2	1	11 210	—	75	—	—
	2	12 565 [1 355]	0.66162	95 [20]	0.68104	1.94%
	3	13 905 [2 695]	1.31592	114 [39]	1.32802	1.21%
	4	15 247 [4 037]	1.97119	133 [58]	1.97501	0.38%
	5	16 399 [5 189]	2.53369	149 [74]	2.51984	1.39%
	6	17 699 [6 489]	3.16846	169 [94]	3.20088	3.24%
	7	18 974 [7 764]	3.79102	188 [113]	3.84786	5.68%
	1	9 862	—	58	—	—
	2	10 672 [810]	0.39551	70 [12]	0.40862	1.31%
	3	11 428 [1 566]	0.76465	81 [23]	0.78319	1.85%
3	4	12 214 [2 352]	1.14844	92 [34]	1.15776	0.93%
	5	12 877 [3 015]	1.47217	101 [43]	1.46423	0.79%
	6	13 622 [3 760]	1.83594	112 [54]	1.83880	0.29%
	7	14 351 [4 489]	2.19189	123 [65]	2.21337	2.15%

(2) The camera is installed on the top of a steel frame near to the trailing beam. When the vehicle approaches the trailing beam, the accuracy of VVSI is affected by the vehicle-induced vibration.[37] (3) The lower resolution and frame rate of the camera will also affect the accuracy of the VVSI. These reasons should be considered to enhance the accuracy of the VVSI detection method when it is utilized as the *priori* information of the MFI method proposed in this study, otherwise, the error of the VVSI detection will compromise the accuracy of moving vehicle load identification.

4.2.2. *MFI results and discussions*

To assess the identified results in this experiment, the relative percentage error between the identified axle-weight w_{iden} and true one w_{true} is defined as follows:

$$RPE_w = \frac{|w_{\mathrm{iden}} - w_{\mathrm{true}}|}{w_{\mathrm{true}}} \times 100\%. \tag{4.3}$$

The MFI results are presented in Table 5 by the proposed method under different combinations of response parameters and vehicle speeds.

In Table 5, bending moment and acceleration responses are represented by "m" and "a", respectively. "1/4", "1/2", "3/4", etc. are sensor locations along the bridge span. For example, "1/2m" represents the bending moment response collected from

Table 5. A comparison on MFI results for different combinations of responses and vehicle speeds.

Response combinations	Speeds/m/s	Front axle weight/kg Identified (True) RPEw	Rear axle weight/kg Identified (True) RPEw	GVW/kg Identified (True) RPEw
3/4m	1.3796	5.8156 (5.5671) 4.46%	5.7560 (5.5717) 3.31%	11.5716 (11.1388) 3.89%
1/2m&3/4m	1.3796	5.4617 (5.5671) 1.89%	5.3047 (5.5717) 4.79%	10.7664 (11.1388) 3.34%
1/2m&3/8a	1.3796	5.0682 (5.5671) 8.96%	5.2720 (5.5717) 5.38%	10.3402 (11.1388) 7.17%
1/2m&3/4m& 3/8a	1.3796	5.2293 (5.5671) 6.77%	5.1820 (5.5717) 6.99%	10.4113 (11.1388) 6.53%
1/2m&3/4m& 3/8a	0.7967	4.9975 (5.5671) 10.23%	5.1183 (5.5717) 8.13%	10.1158 (11.1388) 9.18%

a sensor located at 1/2 span of the bridge. Because only the static axle-weight of the vehicle can be measured directly and the time-varying components of the vehicle are unknown in practice, the static component, which is related to the constant vector of the redundant matrix $\mathbf{\Phi}$ in Eq. (3.10), can be identified by the proposed MFI method and used to calculate the RPEw values here.

From Table 5, it can be found that the proposed method can identify the static weight of the vehicle accurately if only one or two bending moment responses are used for MFI. For the case of "1/2m&3/4m", the RPEw values of the front axle, rear axle and GVW are 1.89%, 4.79% and 3.34%, respectively. Compared with the case of only one response "3/4m", the RPEw value of the GVW decreases with the increase in the response.

Due to the fact that the acceleration response in this experiment is collected by PCB-333B30, its frequency range is from 0.5 Hz to 3 000 Hz,[38] which means that it is difficult to obtain static axle weight of the vehicle if only the acceleration response is used for MFI. Compared with the cases of "3/4m" and "1/2m&3/4m" which only use the bending moment, all the RPEw values increase under the "1/2m&3/8a". One of the reasons is the frequency range of the accelerometer. Another one is that the acceleration responses dominate in a high-frequency domain so that it is easy for them to be polluted by noise. Furthermore, with the introduction of the acceleration response, the dynamic component dominated in the high frequency can be identified accurately. The corresponding comparison on MFI results under the cases of the "1/2m&3/4m" and "1/2m&3/8a" is shown in Fig. 11. It can be found that the fluctuations of the identified results under the "1/2m&3/4m" are relatively small comparing with the ones under the "1/2m&3/8a". This is because the dynamic component is difficult to obtain if only the bending moment is used. With the introduction of the acceleration response, the high-frequency component of the signal is used for MFI. All the MFI results fluctuate around the true static weight which coincides with the *priori* knowledge.[39]

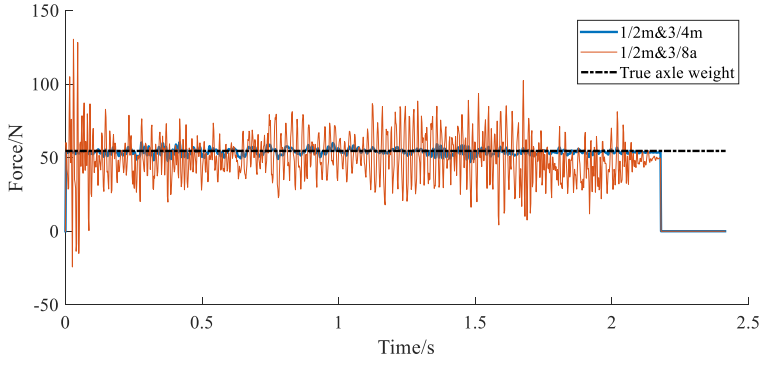

(a)

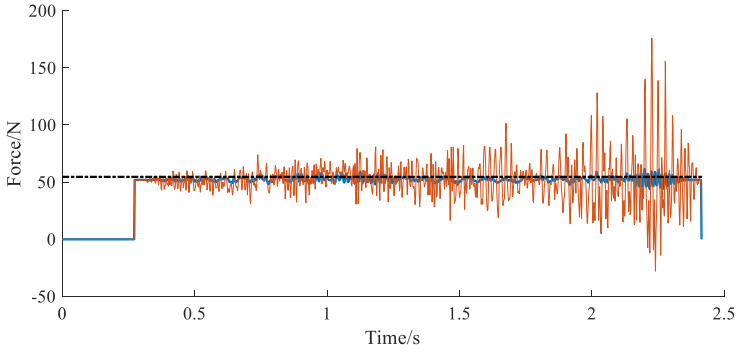

(b)

Fig. 11. Comparing on MFI results from "1/2m&3/4m" and "1/2m&3/8a". (a) First axle. (b) Second axle.

From Table 5, it can also be found that when the vehicle speed decreases to 0.7967 m/s, the RPEw values will increase. One reason is that the system matrix dimension will increase with the increase of the traveling time of vehicle on the bridge and will lead to high computational cost. Another one is that the dimension of the response vector will also be enlarged, and it means that more noise errors are included in the MFI calculation. However, the RPEw values of GVW by the proposed method are still in an acceptable range less than 10%.

To highlight the significance of the introduction of the vision-based vehicle positions in the proposed MFI method, three existing methods are adopted to make a comparative study with the proposed method here. One is a modified time domain method (mTDM), in which the Haar redundant dictionary and Tikhonov regularization adopted are the same as the ones in the proposed method, but it takes the assumption that the vehicle moves across the bridge at a constant velocity as in the traditional TDM.[16] Furthermore, to prove that it is meaningful for

the proposed method to replace the reweighted l_1-norm regularization with the Tikhonov regularization, the identified results by the reweighted l_1-norm regularization method with the same Haar dictionary as in the proposed method, are owing to the so-called the Reweighted L1 method in the following tables and figures. In addition, the MFI problem in Ref. 19 is also solved by the reweighted l_1-norm regularization method but with the redundant dictionary composed of trigonometric and rectangular functions, so it is called the Reweighted L1[19] method in the following tables and figures to distinguish it with the above Reweighted L1 method with the same Haar dictionary as in the proposed method.

In addition, due to the fact that the dynamic component of the vehicle is hard to verify directly, the acceleration at 3/8 span is reconstructed from the MFI results by the proposed method, and it is compared with the measured responses as shown in Fig. 12. One can find that the reconstructed acceleration is closer to the measured one. These observations show that the MFI results obtained by the proposed method are convincible.

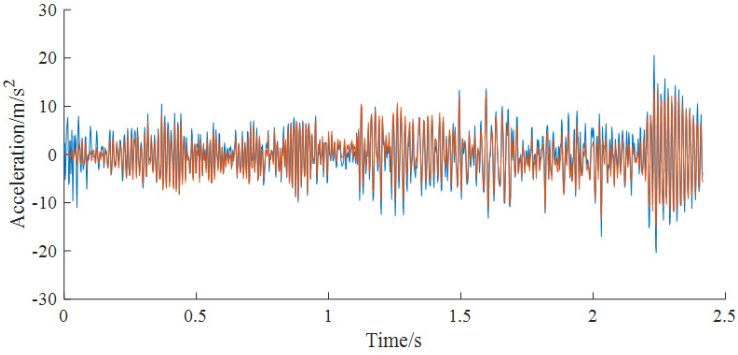

Fig. 12. Comparison on reconstructed and measured acceleration responses from 1/2m&3/4m&3/8a.

Table 6. Comparison on MFI results by different methods under Case 1.

Methods	Front axle weight/kg Identified (True) RPEw	Rear axle weight/kg Identified (True) RPEw	GVW/kg Identified (True) RPEw
mTDM	3.7976 (5.5671) 31.78%	6.4514 (5.5717) 15.79%	10.2490 (11.1388) 7.99%
Reweighted L1	5.5379 (5.5671) 0.52%	4.6662 (5.5717) 16.25%	10.2042 (11.1388) 8.39%
Reweighted L1[19]	4.1089 (5.5671) 26.19%	6.4656 (5.5717) 16.04%	10.5745 (11.1388) 5.07%
Proposed	5.2293 (5.5671) 6.77%	5.1820 (5.5717) 6.99%	10.4113 (11.1388) 6.53%

Furthermore, Table 6 lists the MFI results by different methods under the response combination "1/2m&3/4m&3/8a". Even though the RPEw values on the identified GVW by both the mTDM and the reweighted l_1-norm regularization methods have been controlled in 10%, the RPEw value of each axle is worse than that by the proposed method. For the mTDM method, the RPEw values of the front and rear axles are larger than 15%. Especially for the front axle, the RPEw value attains up to 31.78%. For the reweighted l_1-norm regularization method, even though the RPEw value of the front axle is only 0.52%, the RPEw value of the rear axle is larger than 16%. A comparison on the MFI results obtained by all these methods can be seen in Fig. 13. It can be found that the identified results by the mTDM method fluctuate around the wrong static axle weight. This is because the assumption in the mTDM method that the vehicle speed is unchanged is not according to the real engineering. For the reweighted l_1-norm regularization method, the identified result of the first axle fluctuates around the true axle weight.

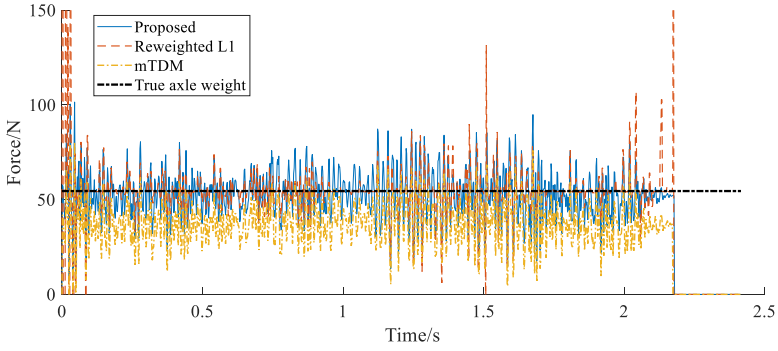

(a)

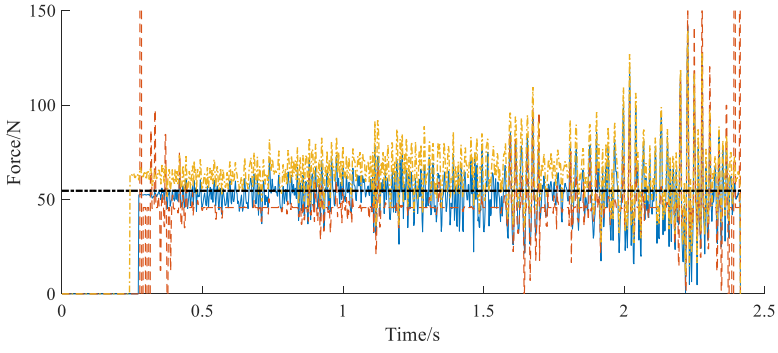

(b)

Fig. 13. Comparing on MFI results from "1/2m&3/4m&3/8a". (a) First axle. (b) Second axle.

However, the identified result of the real axle has a little deviation from the true axle weight. Furthermore, there are significant errors at the moments when the vehicle enters or leaves the beam. Because there are some impulse components at these moments and the sparse recovery solution is still sensitive to them. Therefore, compared with the existing two methods, namely, mTDM and Reweighted L1 regularization, the identified results by the proposed method are more accurate and reasonable.

Compared with the Reweighted L1 method which used the redundant dictionary composed of trigonometric and rectangular functions, it can be found that even though the RPEw value on the identified GVW is only 5.07%, the error of the identified static weight for each axle is large especially for the first axle. Figure 14 also shows the comparison on MFI results by both the proposed method and the Reweighted L1[19] method. It can be found that the identified time histories at the front and rear axles of the moving vehicle by the Reweighted L1[19] method fluctuate

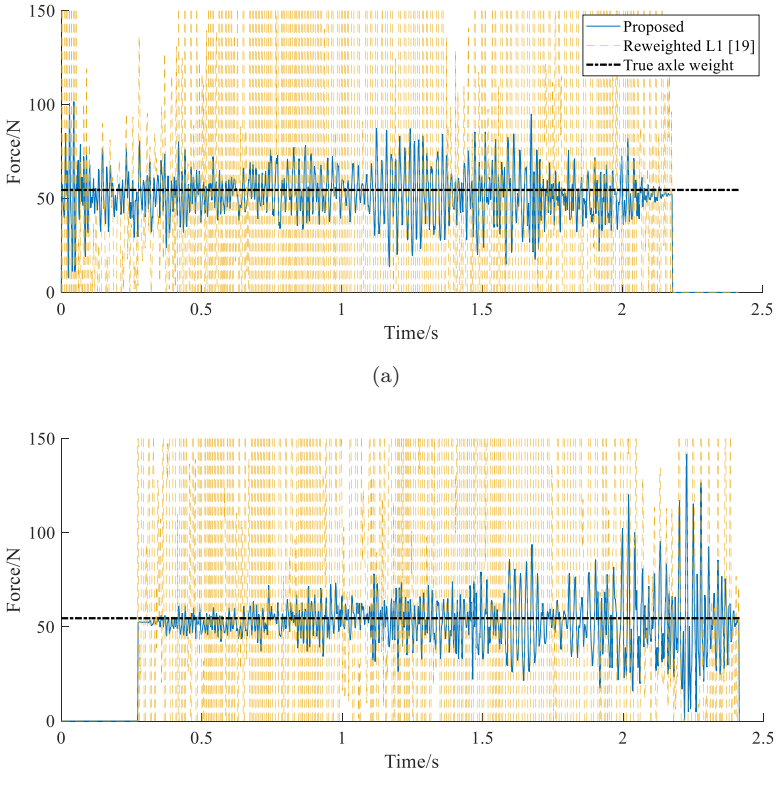

(a)

(b)

Fig. 14. Comparing on MFI results from "1/2m&3/4m&3/8a". (a) First axle. (b) Second axle.

seriously in the whole-time domain. This is because the RPEw value is calculated by the coefficient of the first atom in the redundant matrix which is related to the constant vector in Eq. (3.10). But the time histories of the vehicle are calculated by Eq. (3.8) which consists of all the atoms. And each trigonometric function in the Reweighted L1[19] method is distributed throughout the whole domain and the component dominated in the high-frequency domain is easily polluted by the noise especially when the acceleration response is used. In short, these observations show that the Haar dictionary and the Tikhonov method are the better choices compared with the existing three methods and the proposed method can be applied widely to identify the moving vehicle loads.

5. Conclusions

In this study, a novel MFI method based on TDM is proposed by combining VVSI and vehicle-induced bridge responses. A novel VVSI method combining background subtraction with template matching is presented to detect and track the vehicle accurately. An improved MFI is developed based on the MFI equation reformed in time domain by the instantaneous VVSI instead of the constant speed vehicle crossing bridges assumed in the traditional TDM and based on the redundant dictionary matrix composed of Haar functions for a moving force. The MFI problem is then converted into a solution to atom vectors and then solved by the Tikhonov method. Some experimental verifications and comparative studies are conducted in the laboratory to evaluate the feasibility of the proposed method and some conclusions can be drawn as follows:

(1) The proposed MFI method can effectively identify the moving vehicle loads with a higher and acceptable accuracy, either from the view of the axle-weight and dynamic components of a vehicle load or from the gross weight vehicle (GVW). This shows that it is successful to replace the constant speed vehicle crossing bridges assumed in the traditional TDM with the instantaneous VVSI in the MFI problem. The Haar redundant dictionary adopted here is effective to represent the moving forces when the combined responses of bending moments and accelerations are used to identify the moving forces.
(2) Based on the proposed VVSI method combining the template matching method with the background subtraction method, the computational cost of the template matching method is saved and the influence of background interference on the background subtraction method is reduced. The moments when the vehicle enters or leaves the bridge can be captured accurately and the vehicle can be effectively detected. However, only one vehicle is considered on the bridge deck as a preliminary attempt in this regard, but multiple vehicle scenarios are in general in practice. Furthermore, the vehicle type is known by default in this study so that the wheelbase can be obtained directly. With the increase in

vehicle types in practice, the problem will be bound to become difficult, which should be focused on for good tackling in the future.

(3) The experimental results show that the dynamic components of a vehicle load can be identified easily with the introduction of the acceleration responses into the vehicle-induced combined responses of bridges.

(4) The proposed MFI method can provide more stable and reasonable MFI results compared with the existing three methods. The Haar dictionary is more suitable in the study and the MFI results will be more accurate when it is combined with the Tikhonov method. However, even though the proposed method has a higher accuracy compared with the existing methods, the road roughness in the real engineering may have a great impact on the proposed method, which should be verified in the future.

(5) The proposed VVSI method still needs to be enhanced in the future so that the DOV can be detected more accurately. In addition, the dynamic components of the vehicle loads are hard to validate their accuracy due to the fact that the real dynamic components are hard to measure directly in practice, which is also before us in the future. Furthermore, the experiment model in this study is still simple, and it should be improved in the future to simulate the multiple vehicles and multiple lanes scenarios.

Acknowledgments

This work was jointly supported by the National Natural Science Foundation of China under grant numbers 52178290 and 51678278.

ORCID

Ling Yu https://orcid.org/0000-0002-0139-0966

References

1. H. C. Zhou, H. N. Li, D. H. Yang and T. H. Yi, Development of moving force identification for simply supported bridges: A comprehensive review and comparison, *Int. J. Struct. Stab. Dyn.* **22**(12) (2022) 2230003.
2. X. Q. Zhu and S. S. Law, Recent developments in inverse problems of vehiclebridge interaction dynamics, *J. Civil Struct. Health Monit.* **6**(1) (2016) 107–128.
3. W. Y. He, S. Y. Zhu and Z. W. Chen, A multi-scale wavelet finite element model for damage detection of beams under a moving load, *Int. J. Struct. Stab. Dyn.* **18**(6) (2018) 1850078.
4. H. Shokravi, N. Bakhary, M. Heidarrezaei, S. S. R. Koloor and M. Petru, Vehicle-assisted techniques for health monitoring of bridges, *Sensors* **20**(12) (2020) 3460.
5. Y. B. Yang, Z. L. Wang, K. Shi, H. Xu and Y. T. Wu, State-of-the-art of vehicle-based methods for detecting various properties of highway bridges and railway tracks, *Int. J. Struct. Stab. Dyn.* **20**(13) (2020) 2041004.

6. D. H. Dan, L. F. Ge and X. F. Yan, Identification of moving loads based on the information fusion of weigh-in-motion system and multiple camera machine vision, *Measurement* **144** (2019) 155–166.
7. J. Y. Zheng, J. Y. Tang, Z. X. Zhou, J. L. Heng, X. Chu and T. Wu, Intelligent cognition of traffic loads on road bridges: From measurement to simulation — A review, *Measurement* **200** (2022) 111636.
8. Z. C. Chen, H. Li, Y. Q. Bao, N. Li and Y. Jin, Identification of spatio-temporal distribution of vehicle loads on long-span bridges using computer vision technology, *Struct. Control Health Monit.* **23**(3) (2016) 517–534.
9. L. F. Ge, D. H. Dan and H. Li, An accurate and robust monitoring method of full-bridge traffic load distribution based on YOLO-v3 machine vision, *Struct. Control Health Monit.* **27**(12) (2020) e2636.
10. X. D. Jian, Y. Xia, Jose A. Lozano-Galant and L. M. Sun, Traffic sensing methodology combining influence line theory and computer vision techniques for girder bridges, *J. Sens.* **2019** (2019) 3409525.
11. G. Yang, P. Wang, W. S. Han, S. Z. Chen, S. Y. Zhang and Y. G. Yuan, Automatic generation of fine-grained traffic load spectrum via fusion of weigh-in-motion and vehicle spatial–temporal information, *Comput.-Aided Civil Infrastruct. Eng.* **37**(4) (2022) 485–499.
12. J. S. Zhu, X. T. Li, C. Zhang and T. Shi, An accurate approach for obtaining spatiotemporal information of vehicle loads on bridges based on 3D bounding box reconstruction with computer vision, *Measurement* **181** (2021) 109657.
13. Y. Zhou, Y. L. Pei, S. Zhou, Y. Zhao, J. X. Hu and W. J. Yi, Novel methodology for identifying the weight of moving vehicles on bridges using structural response pattern extraction and deep learning algorithms, *Measurement* **168** (2021) 108384.
14. C. O'Connor, Wheel loads from bridge strains: Laboratory studies, *J. Struct. Eng. New York* **114**(8) (1988) 1724–1740.
15. T. H. T. Chan, S. S. Law, T. H. Yung and X. R. Yuan, An interpretive method for moving force identification, *J. Sound Vib.* **219**(3) (1999) 503–524.
16. S. S. Law, T. H. T. Chan and Q. H. Zeng, Moving force identification: A time domain method, *J. Sound Vib.* **201**(1) (1997) 1–22.
17. S. S. Law, T. H. T. Chan and Q. H. Zeng, Moving force identification — a frequency and time domains analysis, *J. Dyn. Syst. Measur. Control* **121**(3) (1999) 394–401.
18. H. C. Zhou, H. N. Li, D. H. Yang and T. H. Yi, Moving force identification of simply supported bridges through the integral time domain method, *J. Sound Vib.* **534** (2022) 117046.
19. C. D. Pan, L. Yu, H. L. Liu, Z. P. Chen and W. F. Luo, Moving force identification based on redundant concatenated dictionary and weighted l(1)-norm regularization, *Mech. Syst. Signal Process.* **98** (2018) 32–49.
20. H. L. Liu, L. Yu, Z. W. Luo and C. D. Pan, Compressed sensing for moving force identification using redundant dictionaries, *Mech. Syst. Signal Process.* **138** (2020) 106535.
21. B. J. Qiao, Z. Mao, J. X. Liu, Z. B. Zhao and X. F. Chen, Group sparse regularization for impact force identification in time domain, *J. Sound Vib.* **445** (2019) 44–63.
22. Z. H. Zhang, W. Y. He and W. X. Ren, Moving force identification based on learning dictionary with double sparsity, *Mech. Syst. Signal Process.* **170** (2022) 108811.
23. Y. Chu and W.-H. Fang, An efficient approach for the harmonic retrieval problem via Haar wavelet transform, *IEEE Signal Process. Lett.* **4**(12) (1997) 331–333.

24. H. L. Liu, C. Li, L. Yu, Y. F. Wang and J. W. Zhong, Onsite identification of moving vehicle loads on multispan continuous bridge using both dictionary expansion and sparse regularization, *J. Aerospace Eng.* **34**(3) (2021) 04021018.
25. Y. X. Li, L. Sun, M. Y. Xia, L. X. Luo, A. Wang and X. D. Jian, General Tikhonov regularization-based load estimation of bridges considering the computer vision-extracted prior information, *Struct. Control Health Monit.* **29**(12) (2022) e3135.
26. C. Wang, Q. X. Yang, T. Y. Qi and W. X. Ren, A combined method for vehicle load identification based on machine vision and BP neural network, *J. Civil Struct. Health Monit.* **13** (2023) 1061–1075.
27. B. Zhang, L. M. Zhou and J. Zhang, A methodology for obtaining spatiotemporal information of the vehicles on bridges based on computer vision, *Comput.-Aided Civil Infrastruct. Eng.* **34**(6) (2019) 471–487.
28. C. Y. Li, C. Wang, Q. X. Yang and T. Y. Qi, Identification of vehicle loads on an orthotropic deck steel box beam bridge based on optimal combined strain influence lines, *Appl. Sci.-Basel* **12**(19) (2022) 9848.
29. Z. Y. Zhang, Flexible camera calibration by viewing a plane from unknown orientations, in *Proc. Seventh IEEE Int. Conf. Computer Vision* (IEEE, Kerkyra, Greece, 1999), pp. 666–673.
30. X. D. Jian, Z. L. Lai, Y. Xia and L. M. Sun, A robust bridge weigh-in-motion algorithm based on regularized total least squares with axle constraints, *Struct. Control Health Monit.* **29**(10) (2022) e3014.
31. R. S. Stanković and B. J. Falkowski, The Haar wavelet transform: Its status and achievements, *Comput. Elect. Eng.* **29**(1) (2003) 25–44.
32. M. Karpovsky, *Finite Orthogonal Series in the Design of Digital Devices* (John Wiley & Son, New York, 1976), p. 251.
33. A. N. Tikhonov, On the solution of ill-posed problems and the method of regularization, *Dokl. Akad. Nauk SSSR* **151**(3) (1963) 501–504.
34. Z. W. Luo and L. Yu, Regularization strategies for contiguous and noncontiguous damage detection of structures, *Int. J. Comput. Methods* **18**(6) (2021) 2140001.
35. P. C. Hansen, Regularization tools version 4.0 for matlab 7.3, *Numer. Algorithms* **46**(2) (2007) 189–194.
36. B. H. Xu and L. Yu, A novel regularized adaptive matching pursuit for moving force identification using multiple criteria and prior knowledge, *Int. J. Struct. Stab. Dyn.* **23**(10) (2023) 2350117.
37. Z. W. Chen, Y. L. Feng, Y. Zhang, J. T. Liu, C. X. Zhu and A. Chen, An accurate and convenient method of vehicle spatiotemporal distribution recognition based on computer vision, *Sensors* **22**(17) (2022) 6437.
38. Z. W. Chen, W. B. Yang, J. Li, T. H. Yi, J. C. Wu and D. D. Wang, Bridge influence line identification based on adaptive B-spline basis dictionary and sparse regularization, *Struct. Control Health Monit.* **26**(6) (2019) e2355.
39. T. Pinkaew, Identification of vehicle axle loads from bridge responses using updated static component technique, *Eng. Struct.* **28**(11) (2006) 1599–1608.